Connexin50 hemichannels are opened by CO_2: implications for lens physiology

Alexandra Lovatt, Ashvini Wijayapala, Macy Mui, Jack Butler and Nicholas Dale*

School of Life Sciences
University of Warwick
Coventry, CV4 7AL

*Author for correspondence, N.E.Dale@warwick.ac.uk

Key words: connexin; hemichannel; microcirculation; lens fibre cells

Abstract

Connexin50 (Cx50) is expressed in lens fibre cells. As mutations of Cx50 cause cataracts its physiological role in the lens must be important. We have used recent cryoEM structures of Cx50 and the predictive power of alphafold3 to identify the presence of a carbamylation motif, originally described in Cx26, that suggests that Cx50 might be CO_2 sensitive. By expressing the naturally truncated version of Cx50 in HeLa cells and utilising coexpression of genetically encoded sensors iGluSnFr or eLACCO1.1, we have demonstrated the CO_2 sensitivity of Cx50 hemichannels, and their permeability to lactate and glutamate. Importantly, the properties of Cx50 predict that it will be partially open at the levels of PCO_2 characteristic of aqueous humour. By mutating the two key residues of the carbamylation motif, K105 and K140, we have shown that the motif is required for CO_2 sensitivity. Mutations of the residue V44 cause cataracts and these mutations abolish the CO_2 sensitivity of Cx50. We hypothesize that CO_2-dependent gating of Cx50, and consequent alterations in transmembrane Na^+ fluxes, might provide homeostatic control of the microcirculation system that is critical for lens health.

Introduction

Connexin50 (Cx50) is an alpha connexin that shares considerable sequence homology and structural similarity to Cx46 (Myers *et al.*, 2018; Flores *et al.*, 2020). Both Cx50 and Cx46 are part of the alpha connexin clade which also includes Cx43 (Cruciani & Mikalsen, 2006). These three connexins are all expressed in the mammalian lens (Mathias *et al.*, 2010; Berthoud & Ngezahayo, 2017). While Cx43 is found only in the lens epithelium, Cx46 and Cx50 form gap junctions between the lens epithelial and lens fibre cells, and between lens fibre cells. Cx50 is also present in lens fibre cells in the form of hemichannels -unopposed hexameric channels that open into the extracellular space.

To maintain transparency, the lens does not have a blood supply (Mathias *et al.*, 1997). Essential nutrients and metabolic waste products are supplied/removed via a microcirculation system (Mathias *et al.*, 1997; Mathias *et al.*, 2007; Delamere & Tamiya, 2009). This is powered by Na^+ extrusion from equatorial epithelial cells. The movement of Na^+ ions through the gap junction coupled network of lens cells drags along water and other solutes. Water and these solutes re-enter the lens at the poles through the expanded extracellular space provided by the lens sutures.

An open question remains the pathway by which Na^+ ions enter the lens fibre cells (Mathias *et al.*, 1997) to generate extrusion via the Na^+/K^+ pumps in the epithelial cells and thus the microcirculation. Cx50 has been discounted as the source, because the hemichannels are deemed to be closed and instead an unspecified leak channel has been proposed (Mathias *et al.*, 2007). In this paper we show that Cx50 hemichannels are directly sensitive to gaseous CO_2 which acts via a binding mechanism and motif that we have previously shown in Cx26 (Meigh *et al.*, 2013). The properties of Cx50 show that it will be partially open at levels of PCO_2 that are typical of aqueous humour (Krupin *et al.*, 1980) and this suggests that Cx50 hemichannels have the correct properties to be the source of the Na^+ leak current that underlies the microcirculation.

Materials and Methods

Connexin mutagenesis

A cDNA sequence for the human gene for Cx50 according to accession P48165 truncated to 277 amino acids was synthesised by IDT. This truncation of the human gene is equivalent to the natural age-related truncation at His284 documented for the bovine gene (Wang & Schey, 2009). The cDNA sequence was subsequently subcloned into pCAG-GS-mCherry vector prior to transfection. Point mutations were introduced via Gibson assembly methods. Overlapping primer fragments (IDT) both containing the desired mutation were amplified via PCR. Successful mutagenesis was confirmed using Sanger sequencing (GATC Biotech). All Cx50 constructs were inserted upstream of an mCherry tag, linked via a 12 AA linker (GVPRARDPPVAT).

Cell culture and transfection

Parental HeLa DH cells (ECACC 96112022, RRID:CVCL_2483) were cultured with low-glucose DMEM (Merck Life Sciences UK Ltd, CAT# D6046) supplemented with 10% foetal bovine serum

(Labtech.com, CAT# FCS-SA) and 5% penicillin/streptomycin. Cells were seeded onto coverslips at a density of $4x10^4$ cells per well. Cells were transiently transfected to co-express a Cx50 variant and one of the following genetically encoded fluorescent sensors:

pCMV(MinDis).iGluSnFR was a gift from Loren Looger (Addgene plasmid # 41732 ; http://n2t.net/addgene:41732 ; RRID:Addgene_41732) (Marvin *et al.*, 2013).

pAEMXT-eLACCO1.1 was a gift from Robert Campbell (Addgene plasmid # 167946 ; http://n2t.net/addgene:167946 ; RRID:Addgene_167946) (Nasu *et al.*, 2021). To improve expression of eLACCO1.1, this construct was subcloned into the iGluSnFR expression vector backbone. Sequences were verified with Sanger sequencing (GATC).

To transfect cells, a mixture of 1µg of DNA from pCAG-Cx-mCherry construct and 1µg sensor DNA with 3µg PEI was added to cells for 4-8h. Cells were imaged 48h after transfection.

aCSF

Control (20 mmHg PCO_2): 140 mM NaCl, 10 mM $NaHCO_3$, 1.25 mM NaH_2PO_4, 3mM KCl, 1 mM $MgSO_4$.

Control (35 mmHg PCO_2): 124 mM NaCl, 26 mM $NaHCO_3$, 1.25 mM NaH_2PO_4, 3mM KCl, 1 mM $MgSO_4$.

Hypercapnic (55 mmHg PCO_2): 100 mM NaCl, 50 mM $NaHCO_3$, 1.25 mM NaH_2PO_4, 3 mM KCl, 1 mM $MgSO_4$.

Hypercapnic (70 mmHg PCO_2): 70 mM NaCl, 80 mM $NaHCO_3$, 1.25 mM NaH_2PO_4, 3 mM KCl, 1 mM $MgSO_4$.

High K^+ (20 mmHg PCO_2): 93 mM NaCl, 10 mM $NaHCO_3$, 1.25 mM NaH_2PO_4, 50mM KCl, 1 mM $MgSO_4$.

10 mM D-glucose and 2 mM $CaCl_2$ was added to all solutions just before use. Solutions were and saturated with: 98%O_2/2% CO_2 (20 mmHg); 95% O_2/5% CO_2 (carbogen) (35 mmHg), or carbogen plus addtional CO_2 (55 mmHg and 70 mmHg). The amounts of CO_2 were adjusted so that all solutions had a pH of ~7.4.

Live cell fluorescence imaging and analysis

48 hours after transfection, cells were perfused with control aCSF (20 mmHg) until a stable baseline was reached, before switching to either hypercapnic or high K^+ aCSF. Once a stable baseline was reached after solution change, cells were returned to perfusion with control aCSF (20 mmHg). Recordings were calibrated by application of 3 µM of the corresponding analyte.

All cells were imaged by epifluorescence (Scientifica Slice Scope, Cairn Research OptoLED illumination, 60x water Olympus immersion objective, NA 1.0, Hamamatsu ImagEM EM-SSC camera, Metafluor software). cpGFP in the sensors were excited by a 470 nm LED, with emission captured between 504-543 nm. Connexin constructs have a C-terminal mCherry tag, which was excited by a 535 nm LED and emission captured between 570-640 nm. Only cells expressing both cpGFP and mCherry were selected for recording, with cpGFP images acquired

every 4 seconds. For each condition, at least 3 independent transfections were performed with at least 2 coverslips per transfection.

Analysis of all experiments was carried out in ImageJ. Images were opened as a stack and stabilised for movement (Li, 2008). ROIs were drawn around cells co-expressing both sensor and connexin. Median pixel intensity was plotted as normalised fluorescence change ($\Delta F/F_0$) over time to give traces of fluorescence change. The amount of analyte release was quantified as concentration by normalising to the $\Delta F/F_0$ caused by application of 3 μM of analyte, which was within the linear portion of the dose response curve for each sensor.

Statistical analysis

Each cell was considered as an independent replicate. All quantitative data is presented as box and whisker plots, where the line represents the median, the box is the interquartile range, and the whiskers are the range, with all individual data points included. Non-parametric statistical tests were used: the Kruskal Wallis ANOVA and the Mann Whitney *U*-test. All calculations were performed on GraphPad Prism.

Results

Cx50 possesses the carbamylation motif and is CO_2 sensitive

Alignment of the Cx50 sequence with that of Cx26 and Cx43, both of which are CO_2 sensitive (Huckstepp *et al.*, 2010; Meigh *et al.*, 2013; Dospinsecu *et al.*, 2025) revealed the presence of the carbamylation motif $_{140}$KFRLEGT$_{146}$ in Cx50. This sequence is analogous to the motifs of $_{144}$KVKMRGG$_{150}$ in Cx43 and $_{125}$KVRIEGS$_{131}$ in Cx26. The carbamylation motif is within the cytoplasmic loop, which has proven to be notoriously difficult to resolve in cryoEM structures for all connexins (Maeda *et al.*, 2009; Myers *et al.*, 2018; Flores *et al.*, 2020; Lee *et al.*, 2020; Brotherton *et al.*, 2022; Qi *et al.*, 2023; Brotherton *et al.*, 2024). Experimental Cx50 structures (e.g. 7JJP) show that K105 is in a similar orientation as K105 of Cx43 and R104 of Cx26. These latter residues form a salt bridge with the carbamylated Lys residue from the neighbouring subunit. Understanding the location of K140 is more difficult. The alphafold3 prediction for the cytoplasmic loop and the position of K140 is of low confidence and experimental structures do not resolve the entire cytoplasmic loop. However, some structures (e.g. 7JM9), while not resolving K140, do place R142 close to its location in the alphafold3 prediction suggesting that the predicted positioning of K140 is likely to be approximately correct. Therefore, there is a reasonable probability that K140 is sufficiently close to K105 to form an inter-subunit salt bridge following carbamylation of K140.

As Cx50 appears to have the carbamylation motif, we tested its CO_2 sensitivity by expressing Cx50 in HeLa DH cells. To assay hemichannel opening we measured the possible efflux of either glutamate or lactate via Cx50 by co-expressing the genetically encoded sensors iGluSNFR or eLACCO1.1. We used these sensors as opposed to the more obvious use of $GRAB_{ATP}$ to assay ATP release (Butler & Dale, 2023), as we found in exploratory experiments that Cx50 hemichannels are not permeable to ATP (Lovatt et al 2025).

Parental HeLa cells that expressed only iGluSnFr or eLACCO1.1 did not exhibit fluorescence changes in response to hypercapnic and depolarising stimuli (Fig 1). To test the possible CO_2-

sensitivity of Cx50, we next co-expressed this connexin with each of the genetically encoded sensors. Starting at a PCO_2 of 20 mmHg, we successively switched to 35, 55 and 70 mmHg PCO_2 solutions. We observed CO_2-dependent fluorescence changes for both analytes (Fig 2). We therefore conclude that Cx50 is CO_2 sensitive and will permit CO_2-dependent efflux of glutamate and lactate. Interestingly, significant release of glutamate and lactate was observed at a PCO_2 of 35 mmHg. Maximal glutamate and lactate release was observed at a PCO_2 of 55 mmHg and some inhibition of release, relative to this maximum, was observed at a PCO_2 of 70 mmHg (Fig 2C,D).

The CO_2-sensitivity of Cx50 depends on the carbamylation motif

We next tested whether the observed CO_2 sensitivity of Cx50 depended on K140 and K105 by individually mutating these residues to Gln. Gln cannot be carbamylated and, being neutral, will not be able to form a salt bridge with a carbamylated Lys residue. Application of 55 mmHg PCO_2 solutions to HeLa cells expressing either $Cx50^{K140Q}$ or $Cx50^{K105Q}$ was ineffective at evoking glutamate release (Fig 3). As a positive control to demonstrate the presence of functional hemichannels, we used 50 mM KCl to depolarise the HeLa cells. This stimulus gave robust glutamate release showing that the mutated channels remained voltage sensitive and permeable to glutamate (Fig 3). We conclude that the action of CO_2 in opening Cx50 hemichannels depends upon the carbamylation motif that we had previously identified in its structure.

Some cataract forming mutations of Cx50 alter its CO_2-sensitivity

Cx50 plays a key role in the physiology of the lens and certain mutations cause cataract formation (Shiels *et al.*, 1998; Berthoud & Ngezahayo, 2017; Berthoud *et al.*, 2020; Shiels & Hejtmancik, 2021; Shi *et al.*, 2022). We have examined whether three of these mutations V44A, V44E, W45S alter CO_2 sensitivity (Fig 4). We found that both mutations of V44 abolished the CO_2 sensitivity of Cx50 hemichannels, but the mutated channels remained voltage sensitive and permeable to glutamate. However, $Cx50^{W45S}$ hemichannels remained CO_2 sensitive but significantly less so than $Cx50^{WT}$ ($p<0.0001$, Fig 4). Our results raise the possibility that loss or reduction of CO_2 sensitivity of Cx50 could be a contributing cause to cataract formation.

To check whether the results of the mutations could be explained by altered membrane localisation, we stained the plasma membrane with DiO and examined colocalization of DiO with the mCherry tag on Cx50 for the WT channel and all mutated variants (Fig 5). This analysis showed that the Manders' coefficients were the same for all Cx50 variants. Thus, the mutations did not alter membrane localisation of Cx50.

Discussion

Cx50 is the fifth connexin, after Cx26, Cx30, Cx32 and Cx43, that is now known to be CO_2 sensitive. Significantly, it is the second alpha connexin alongside Cx43 that has this property. All 5 connexins share a carbamylation motif that was originally identified in Cx26 and the beta connexins. The mechanism of CO_2 dependent hemichannel opening in Cx43 involves 4 Lys residues: K105, K109, K144 and K234 (Dospinsecu *et al.*, 2025). Cx50 lacks K109 (this residue is an Arg) and it is interesting that mutation of either K105 or K140 in Cx50 is sufficient to abrogate CO_2 sensitivity. In Cx43 at least 2 Lys residues must be mutated to abolish CO_2 sensitivity (Dospinsecu *et al.*, 2025). Thus, the mechanism of CO_2 sensitivity in Cx50 is somewhat simpler than in the related Cx43 and more like that proposed for Cx26 (Meigh *et al.*, 2013; Brotherton *et al.*, 2022; Brotherton *et al.*, 2024).

The properties of Cx50 appear to be matched to the physiology of the lens. Firstly, it is significantly open at a PCO_2 of 35 mmHg. PCO_2 of aqueous humour is generally observed as being a little lower than that measured in plasma (Salit, 1930; Krupin *et al.*, 1980; Sharma *et al.*, 1983) and is in the range 35-40 mmHg. We therefore predict that Cx50 hemichannels will be partially open and provide a continual source of Na^+ ions to power the microcirculation. Secondly the degree of opening of Cx50 will be proportional to PCO_2 over the relevant physiological range. We propose the hypothesis that CO_2 acting via Cx50 could mediate homeostatic control of microcirculation. Under this hypothesis, were PCO_2 to rise above its normal resting level, it would imply insufficient microcirculation and waste removal. As a consequence of the increased PCO_2, Cx50 hemichannels would open more and allow a greater Na^+ influx leading to faster microcirculation and a corrective adaptive response. Conversely, if PCO_2 were to fall below the normal resting level, it would imply that the microcirculation was too fast. Cx50 hemichannels would close in response to the lowered PCO_2, reducing the Na^+ influx and hence the rate of microcirculation once again leading to a corrective adaptive response. Direct experimental evidence is required to test this hypothesis, such as whether the rate of microcirculation in the lens can be altered in a CO_2-dependent manner that is consistent with the properties of Cx50.

Thirdly, Cx50 hemichannels are permeable to lactate. To maintain transparency of the lens, as lens fibre cells mature, they lose their organelles including mitochondria (Bassnett, 2002). This means that they become dependent on ATP supply from more metabolically active cells via gap junctions and from glycolysis. Lactate is the end product of glycolysis and thus the permeability of Cx50 to lactate potentially provides an effective way of allowing efflux from the fibre cells of this end product.

We have previously shown that a subset of pathological mutations of Cx26, Cx32 and Cx43 that respectively cause keratitis ichthyosis deafness syndrome (KIDS), X-linked Charcot Marie Tooth Disease (CMTX) and oculodentodigital dysplasia (ODDD) abolish the CO_2 sensitivity of these hemichannels (Meigh *et al.*, 2014; de Wolf *et al.*, 2016; Cook *et al.*, 2019; Butler & Dale, 2023; Dospinsecu *et al.*, 2025). Our observation that some cataract-forming mutations of Cx50 also modify its CO_2 sensitivity therefore fits this pattern. Our observation is consistent with, but does not substantiate, the hypothesis that the loss of CO_2 sensitivity of Cx50 contributes to cataract formation. As $Cx50^{W45S}$ retains reduced CO_2-sensitivity yet also causes cataracts, loss of other properties of Cx50 must also contribute to cataract formation. Clearly, examination of further

cataract mutations will be required to understand any potential role that loss of CO_2 sensitivity might have in the aetiology of cataract formation. In addition, testing whether mutations that directly target CO_2 sensitivity (e.g. K140Q) are sufficient to trigger cataract formation would be a more rigorous test of this hypothesis.

Conflict of interest

The authors declare that there is no conflict of interest

Funding

AL was funded by the Medical Research Council through the University of Warwick Doctoral Training Partnership, grant number MR/N014294/1**.** JB was supported by the Biotechnology and Biological Sciences Research Council (BBSRC) and University of Warwick funded Midlands Integrative Biosciences Training Partnership (MIBTP) grant number BB/T00746X/1.

References

Bassnett, S. (2002) Lens organelle degradation. *Experimental eye research*, **74**, 1-6.

Berthoud, V.M., Gao, J., Minogue, P.J., Jara, O., Mathias, R.T. & Beyer, E.C. (2020) Connexin Mutants Compromise the Lens Circulation and Cause Cataracts through Biomineralization. *Int J Mol Sci*, **21**.

Berthoud, V.M. & Ngezahayo, A. (2017) Focus on lens connexins. *BMC cell biology*, **18**, 6.

Brotherton, D.H., Nijjar, S., Savva, C.G., Dale, N. & Cameron, A.D. (2024) Structures of wild-type and a constitutively closed mutant of connexin26 shed light on channel regulation by CO2. *eLife*, **13**, RP93686.

Brotherton, D.H., Savva, C.G., Ragan, T.J., Dale, N. & Cameron, A.D. (2022) Conformational changes and CO2-induced channel gating in connexin26. *Structure*, **30**, 697-706.

Butler, J. & Dale, N. (2023) X-linked Charcot Marie Tooth mutations alter CO2 sensitivity of connexin32 hemichannels. *Front Cell Neurosci*, **17**, 1330983.

Cook, J., de Wolf, E. & Dale, N. (2019) Cx26 keratitis ichthyosis deafness syndrome mutations trigger alternative splicing of Cx26 to prevent expression and cause toxicity in vitro. *Royal Society open science*, **6**, 191128.

Cruciani, V. & Mikalsen, S.O. (2006) The vertebrate connexin family. *Cell Mol Life Sci*, **63**, 1125-1140.

de Wolf, E., van de Wiel, J., Cook, J. & Dale, N. (2016) Altered CO2 sensitivity of connexin26 mutant hemichannels in vitro. *Physiol Rep*, **4**, e13038.

Delamere, N.A. & Tamiya, S. (2009) Lens ion transport: from basic concepts to regulation of Na,K-ATPase activity. *Experimental eye research*, **88**, 140-143.

Dospinsecu, V.M., Mascarenhas, A., Butler, J., Nijjar, S., de Oliveira Taborda, K., Connors, S., Huang, L. & Dale, N. (2025) CO2-dependent opening of Connexin 43 hemichannels. *bioRxiv*, 2025.2001.2013.632711.

Flores, J.A., Haddad, B.G., Dolan, K.A., Myers, J.B., Yoshioka, C.C., Copperman, J., Zuckerman, D.M. & Reichow, S.L. (2020) Connexin-46/50 in a dynamic lipid environment resolved by CryoEM at 1.9 A. *Nat Commun*, **11**, 4331.

Huckstepp, R.T., Eason, R., Sachdev, A. & Dale, N. (2010) CO2-dependent opening of connexin 26 and related beta connexins. *J Physiol*, **588**, 3921-3931.

Krupin, T., Feitl, M., Roshe, R., Lee, S. & Becker, B. (1980) Halothane anesthesia and aqueous humor dynamics in laboratory animals. *Invest Ophthalmol Vis Sci*, **19**, 518-521.

Lee, H.-J., Jeong, H., Hyun, J., Ryu, B., Park, K., Lim, H.-H., Yoo, J. & Woo, J.-S. (2020) Cryo-EM structure of human Cx31.3/GJC3 connexin hemichannel. *Science Advances*, **6**, eaba4996.

Li, K. (2008) The image stabilizer plugin for ImageJ.

Maeda, S., Nakagawa, S., Suga, M., Yamashita, E., Oshima, A., Fujiyoshi, Y. & Tsukihara, T. (2009) Structure of the connexin 26 gap junction channel at 3.5 A resolution. *Nature*, **458**, 597-602.

Marvin, J.S., Borghuis, B.G., Tian, L., Cichon, J., Harnett, M.T., Akerboom, J., Gordus, A., Renninger, S.L., Chen, T.W., Bargmann, C.I., Orger, M.B., Schreiter, E.R., Demb, J.B., Gan, W.B., Hires, S.A. & Looger, L.L. (2013) An optimized fluorescent probe for visualizing glutamate neurotransmission. *Nat Methods*, **10**, 162-170.

Mathias, R.T., Kistler, J. & Donaldson, P. (2007) The lens circulation. *J Membr Biol*, **216**, 1-16.

Mathias, R.T., Rae, J.L. & Baldo, G.J. (1997) Physiological properties of the normal lens. *Physiol Rev*, **77**, 21-50.

Mathias, R.T., White, T.W. & Gong, X. (2010) Lens gap junctions in growth, differentiation, and homeostasis. *Physiol Rev*, **90**, 179-206.

Meigh, L., Greenhalgh, S.A., Rodgers, T.L., Cann, M.J., Roper, D.I. & Dale, N. (2013) CO2 directly modulates connexin 26 by formation of carbamate bridges between subunits. *eLife*, **2**, e01213.

Meigh, L., Hussain, N., Mulkey, D.K. & Dale, N. (2014) Connexin26 hemichannels with a mutation that causes KID syndrome in humans lack sensitivity to CO2. *eLife*, **3**, e04249.

Myers, J.B., Haddad, B.G., O'Neill, S.E., Chorev, D.S., Yoshioka, C.C., Robinson, C.V., Zuckerman, D.M. & Reichow, S.L. (2018) Structure of native lens connexin 46/50 intercellular channels by cryo-EM. *Nature*, **564**, 372-377.

Nasu, Y., Murphy-Royal, C., Wen, Y., Haidey, J.N., Molina, R.S., Aggarwal, A., Zhang, S., Kamijo, Y., Paquet, M.E., Podgorski, K., Drobizhev, M., Bains, J.S., Lemieux, M.J., Gordon, G.R. & Campbell, R.E. (2021) A genetically encoded fluorescent biosensor for extracellular L-lactate. *Nat Commun*, **12**, 7058.

Qi, C., Acosta Gutierrez, S., Lavriha, P., Othman, A., Lopez-Pigozzi, D., Bayraktar, E., Schuster, D., Picotti, P., Zamboni, N., Bortolozzi, M., Gervasio, F.L. & Korkhov, V.M. (2023) Structure of the connexin-43 gap junction channel in a putative closed state. *eLife*, **12**.

Salit, P.W. (1930) A study of the acid-base equilibrium of the ocular humours. *Biochem J*, **24**, 596-605.

Sharma, R.G., Mishra, Y.C., Verma, G.L. & Lal, K. (1983) A clinical evaluation of oxygen and carbon dioxide values and pH in the human aqueous humour in normal and cataractous eyes. *Indian Journal of Ophthalmology*, **31**.

Shi, Y., Li, X. & Yang, J. (2022) Mutations of CX46/CX50 and Cataract Development. *Frontiers in molecular biosciences*, **9**, 842399.

Shiels, A. & Hejtmancik, J.F. (2021) Inherited cataracts: Genetic mechanisms and pathways new and old. *Experimental eye research*, **209**, 108662.

Shiels, A., Mackay, D., Ionides, A., Berry, V., Moore, A. & Bhattacharya, S. (1998) A missense mutation in the human connexin50 gene (GJA8) underlies autosomal dominant "zonular pulverulent" cataract, on chromosome 1q. *Am J Hum Genet*, **62**, 526-532.

Wang, Z. & Schey, K.L. (2009) Phosphorylation and truncation sites of bovine lens connexin 46 and connexin 50. *Experimental eye research*, **89**, 898-904.

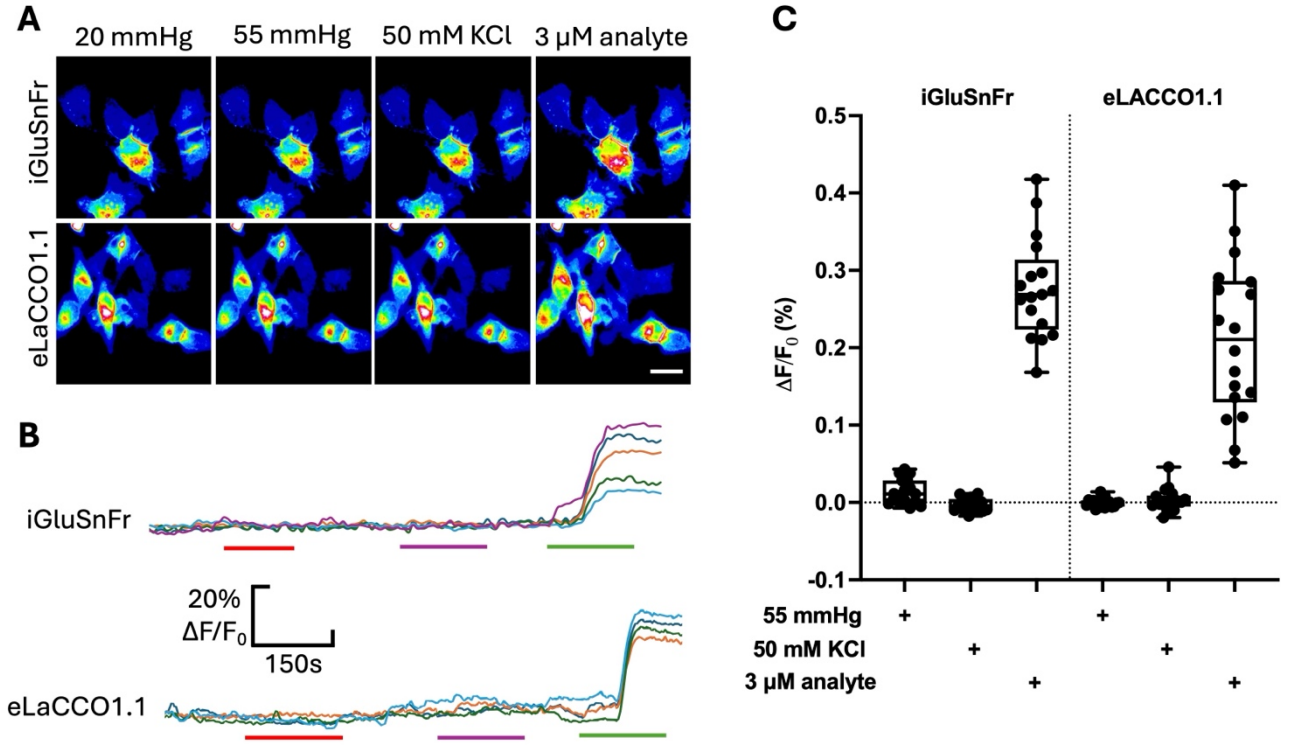

Figure 1. Parental HeLa DH cells do not release either glutamate or lactate in response to hypercapnia or depolarisation. A) Images of iGluSnFr or eLACCO1.1 fluorescence in HeLa cells. No change in fluorescence intensity was seen when the PCO_2 of the aCSF was changed from 20 to 55 mmHg or when 50 mM KCl was applied. Scale bar 20 µm. B) Traces showing the plot of fluorescence changes ($\Delta F/F_0$) versus time for the images in A. Red bar, application of 55 mmHg PCO_2; purple bar, 50 mM KCl; green bar, application of the relevant analyte at 3 µM; all stimuli applied from a baseline of 20 mmHg PCO_2. C) Summary data showing that parental HeLa cells do not show fluorescence changes in response to CO_2 or KCl. Data from 3 transfections each for iGluSnFr and eLACCO1.1.

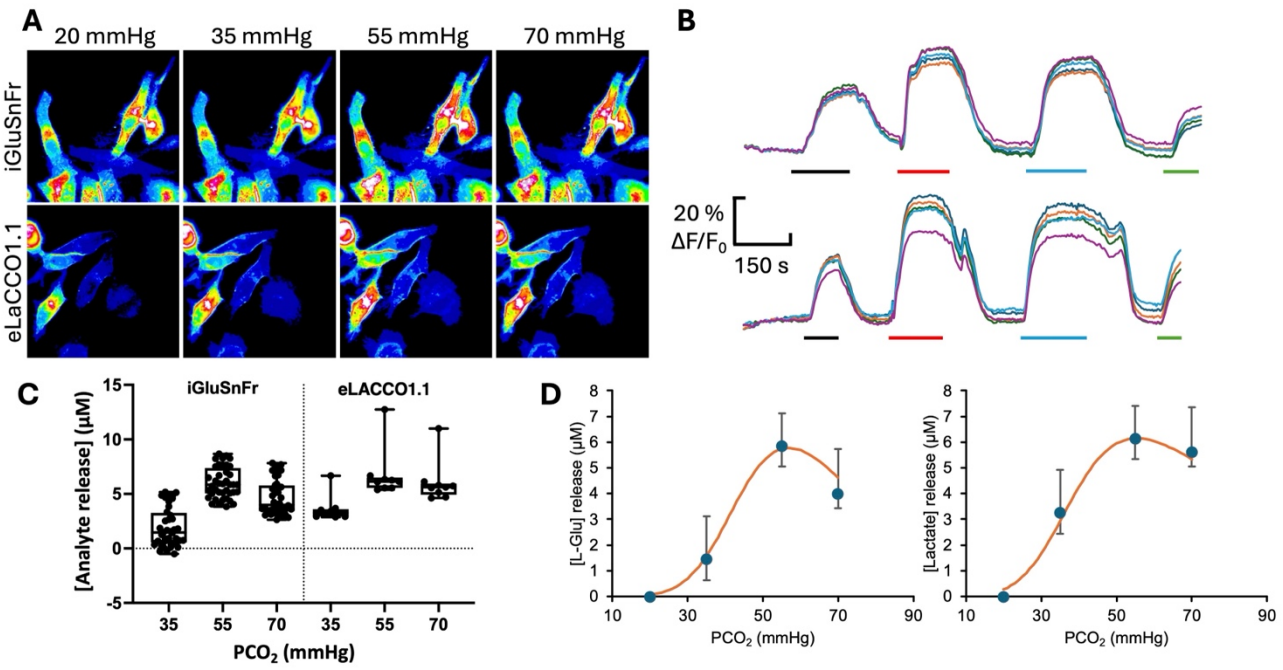

Figure 2. Connexin 50 is CO_2 sensitive. A) Images of iGluSnFr or eLACCO1.1 fluorescence in HeLa cells that express Cx50 to show the progressive larger changes in fluorescence intensity when the PCO_2 of the aCSF was changed from 20 to 35, 55 and 70 mmHg. Scale bar 20 μm. B) Traces showing the plot of fluorescence changes ($\Delta F/F_0$) for iGluSnFr (top) or eLACCO1.1 (bottom) versus time for the images in A during application of 35 mmHg (black bar), 55 mmHg (red bar), 70 mmHg (light blue bar) and 3 μM analyte (green bar). C) Summary data plotted as box and whisker plots showing CO_2 evoked glutamate and lactate release (from four independent transfections for each analyte). D) CO_2-dependent release of glutamate and lactate from Cx50 expressing cells replotted as median with upper and lower quartiles. The continuous line is a modified Hill equation:

$$[A]=Max.\{(C/K)^H/(1+(C/K)^H)\}.\{1-(C/K_i)^{Hi}/(1+(C/K_i)^{Hi})\}$$

Where A is the analyte, C is the partial pressure of CO_2 (mmHg), K and H are the affinity and Hill coefficient of the channel for opening by CO_2, K_i and H_i are the affinity and Hill coefficient for inhibition of the channel by CO_2, and Max (μM) is the asymptotically maximum released concentration of the analytes to CO_2. The parameters for the curves are:

	Glu	**Lac**
H	6	5
K (mmHg)	46	42
Max (μM)	10	11.5
K_i (mmHg)	70	70
H_i	5	3

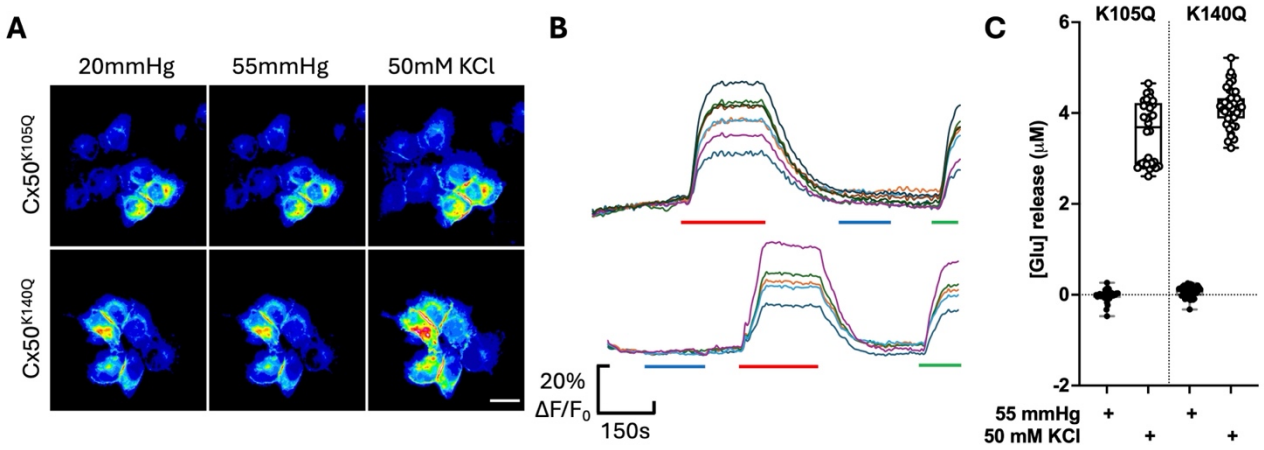

Figure 3. The CO_2 sensitivity of Cx50 depends on the carbamylation motif residues K140 and K105. A) Images of iGluSnFr fluorescence showing that the mutations K105Q and K140Q abolish CO_2-dependent glutamate release from HeLa cells expressing these mutant Cx50 hemichannels. A depolarising stimulus (50 mM KCl) was still able to evoke glutamate release demonstrating that the mutant hemichannels remain voltage dependent and permeable to glutamate. Scale bar 20 μm. B) Traces showing the plot of fluorescence changes ($\Delta F/F_0$) versus time for the images in A. Re bar, application of 55 mmHg PCO_2; purple bar, 50 mM KCl; green bar 3 μM glutamate; all stimuli applied a baseline of 20 mmHg PCO_2. C) Summary data from 4 independent transfections for K105Q and 5 independent transfections of K140Q showing that these mutations abolish the CO_2 evoked glutamate release.

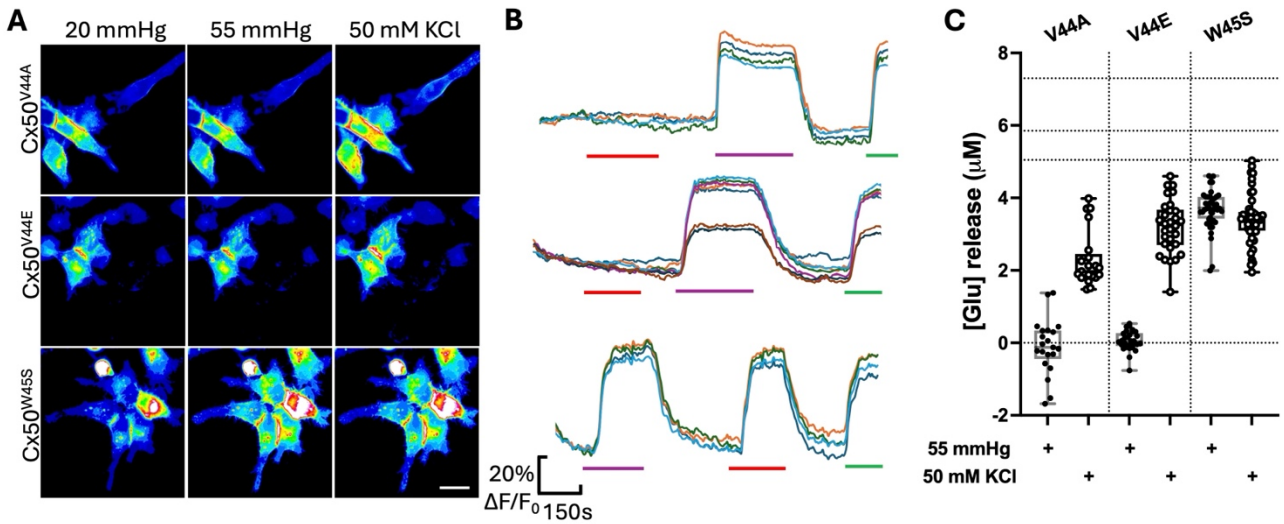

Figure 4. Some cataract forming mutations of Cx50 remove its CO_2 sensitivity. A) Images of iGluSnFr fluorescence showing that the mutations V44E and V44A but not W45S abolish CO_2-dependent glutamate release from HeLa cells expressing these mutant Cx50 hemichannels. A depolarising stimulus (50 mM KCl) is still able to evoke glutamate release demonstrating that the mutant hemichannels remain voltage dependent and permeable to glutamate. Scale bar 20 μm. B) Traces showing the plot of fluorescence changes ($\Delta F/F_0$) versus time corresponding to the images in A. Red bar, application of 55 mmHg PCO_2; purple bar 50 mM KCl; green bar, 3 μM glutamate; all stimuli applied from a baseline of 20 mmHg PCO_2. C) Summary data for: V44A, 4 independent transfections; V44E, 4 independent transfections; and W45S, 5 independent transfections. The dotted lines at top of y-axis show the values for the median CO_2-evoked glutamate release with lower and upper quartiles for $Cx50^{WT}$. $Cx50^{V44A}$ and $Cx50^{V44E}$ are insensitive to CO_2, while $Cx50^{W45S}$ releases significantly less glutamate to 55 mmHg than the wildtype channel (MW Test, $p<0.0001$).

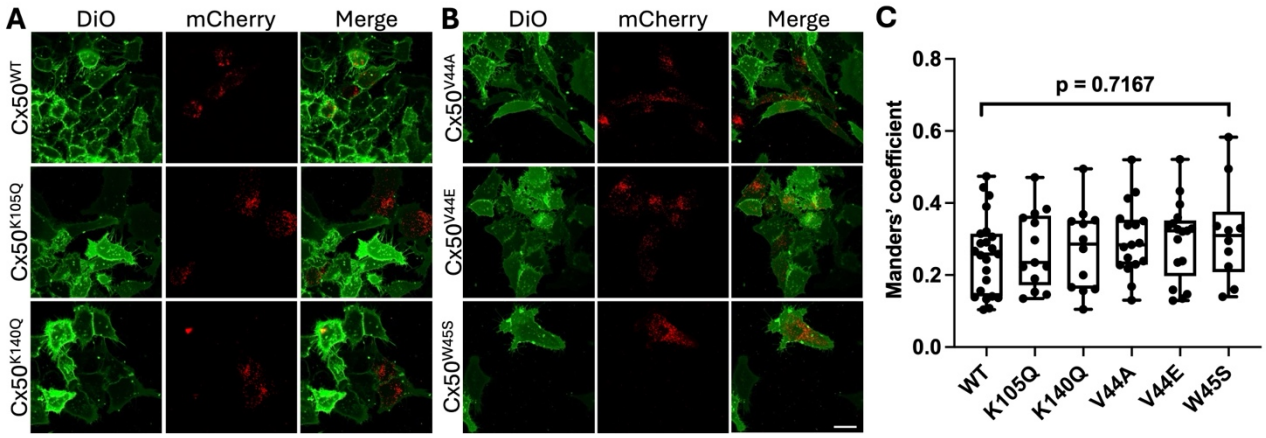

Figure 5. Carbamylation motif mutations and cataract forming mutations do not alter expression of Cx50 at the plasma membrane. A,B) Images showing membrane staining with DiO (green) and the mCherry C-terminal tag on the Cx50 variants (red). Scale bar 20 µm. C) Measurement of the Manders' coefficient (the proportion of DiO fluorescence that colocalises with mCherry) for each Cx50 variant. These coefficients do not differ between the wild type and the mutants (Kruskal Wallis ANOVA, p=0.7167). Data from 3 independent transfections for each variant.